Mining, Metallurgy & Exploration (2022) 39:1821–1832
https://doi.org/10.1007/s42461-022-00605-0

Investigation of Gas and Airflow Distribution in a Block Cave Mine

Yong Pan[1] · **Purushotham Tukkaraja**[1] · **Srivatsan Jayaraman Sridharan**[1]

Received: 12 September 2021 / Accepted: 14 April 2022 / Published online: 12 May 2022

Abstract
Block cave mining method poses unique ventilation challenges compared to other underground metal mining methods. This research study focuses on assessing the airflow behavior in regulated airflow distribution systems by developing a 1:100 scaled block cave experimental model and a numerical model. This study also investigated gas flow behavior under various airflow conditions. Based on our findings, we observed that reduction in particle size and porosity of caved materials, decrease in cave footprint, and closure of undercut drifts would increase cave airflow resistance. The increased airflow is found beneficial for gas dilution regardless of its source locations, while the regulated airflow distribution system might deteriorate gas dilution situation when the source is located in the extraction drifts.

Keywords Airflow distribution · Cave footprint · Cave airflow resistance · Block cave ventilation · CFD · Gas flow characteristics

1 Introduction

Block caving is suitable for mining massive, deep-seated, and low-grade ore deposits. However, the challenges associated with block caving mining such as air blasts, coarse fragmentation, and mud rush should be considered and appropriate mitigation strategies must be planned. In the case of orebodies with uranium mineralization, the extraction of broken rock via drawpoints would cause harmful gases to be released and transported with the main airstream into working areas [1–3].

Additionally, diesel-operated equiment (load haul dump (LHD)) are commonly used in the mechanized mines with higher production targets. A considerable diesel particulate matter (DPM) and dust generated could worsen the underground working environment. Regulations over harmful gases tend to be much stricter than before due to a better understanding of their adverse impacts on human health [4]. Ventilation plays a vital role in reducing adverse gas emission impact. Keeping a negative pressure on the cave by installing multiple fans or regulators is considered common practice to minimize gas concentrations [1]. Ventilation cost could be around 25–50% of total energy consumption dispensed for all activities carried out underground [5]. While under ventilation can result in safety concerns, over ventilation can result in huge operating costs. Optimal ventilation design and fan opereating points are essential for a safe underground environment and economic operation. To design an effective ventilation system, knowledge of the airflow resistance and gas distribution in the system is necessary.

Continuous alteration in cave porosity, irregular geometry, and unique structures complicate investigations of the airflow behavior in a block cave mine [6–8]. Air gap dimensions profoundly affect the cave airflow resistance [9, 10]. Undercut drifts with active ventilation affect airflow resistance within the cave and the extraction levels [11, 12]. Cave sizes differ in various mines from hundreds to thousands of drawpoints; e.g., the E48 cave at the Northparkes mine has 214 drawpoints while the Deep Ore Zone cave at the PT Freeport Indonesia mine contains 1324 drawpoints [13, 14]. Cave size also varies due to the inconsistency of orebody within a single cave [13]. Besides, cave airflow resistance is affected by the numbers and dimensions of airways and orepasses.

Accurate estimation of airflow resistance through porous media is essential. It is common to develop *P*-*Q* (pressure-airflow quantity) curves and $P = RQ^n$ equations to understand airflow characteristics through a porous system. Several research studies have been conducted to investigate

✉ Purushotham Tukkaraja
pt@sdsmt.edu

[1] Department of Mining Engineering and Management, South Dakota Mines, Rapid City, SD, USA 57701

the airflow resistance among agriculture products (porous media), such as walnuts [15], sugarbeet root [16], marigold flowers [17], pistachio nuts [18], chickpea seeds [19], soybeans [20], parchment coffee [21], and poppy seeds [22]; these studies reported that the index *n* value was around 1.8 for uniform airflow through a regular porous media. Baysal et al. [6] and Erogul et al. [9] noted that the airflow pattern observed within a caved zone was different compared to typical mine airways due to unique structure and airflow recirculation in a block cave mine. Besides, a combination of a one-dimensional ventilation software (VENTSIM) and a three-dimensional software (CFD) is relatively a new approach to investigate the airflow behavior and index *n* value in the airflow characteristic equation [23–25].

The gas release rate is affected by its surrounding conditions, such as temperature, moisture content, and porosity of the caved rock; gas source location may vary due to different geological conditions [26]. Previous studies assumed a constant gas generation rate and even distribution of gas concentration in the caved zone [27, 28]; this is not the case in a real-world mine due to the variation of ore grade distribution, and we rarely have the chance to decide the desired geological condition [29]. On-site data confirmed this variation by observing abnormal concentrations associated with orebody deposits [1]. DPM, CO, and dust generated from heavy underground mining equipment operated in the production level should be evaluated to design an effective ventilation system [30–32]. Application of negative pressure on the cave led to roughly 55% and 65% reductions in radon and DPM concentrations [1], respectively, at the Henderson mine; and this technique was also applied to control dust in orepasses [33].

As mentioned above, cave airflow behavior is highly dependent on cave structures (undercut level, air gap, orepass), cave parameters (caved materials properties and footprint), and other elements (fan operation and regulators). It is difficult to investigate the effects of these conditions at a real operating mine. This research focused on investigating the effects of these conditions on cave airflow and gas flow behavior in regulated airflow distribution systems using scaled experimental and computational fluid dynamics (CFD) models.

2 Research Approach

2.1 Experimental Setup

As shown in Fig. 1 and Fig. 2, our scaled block cave model contains a caved zone, an extraction level, an undercut level, drawbells, multiple ducts, and two regulators with

Fig. 2 Nine extraction and three undercut drift inlets

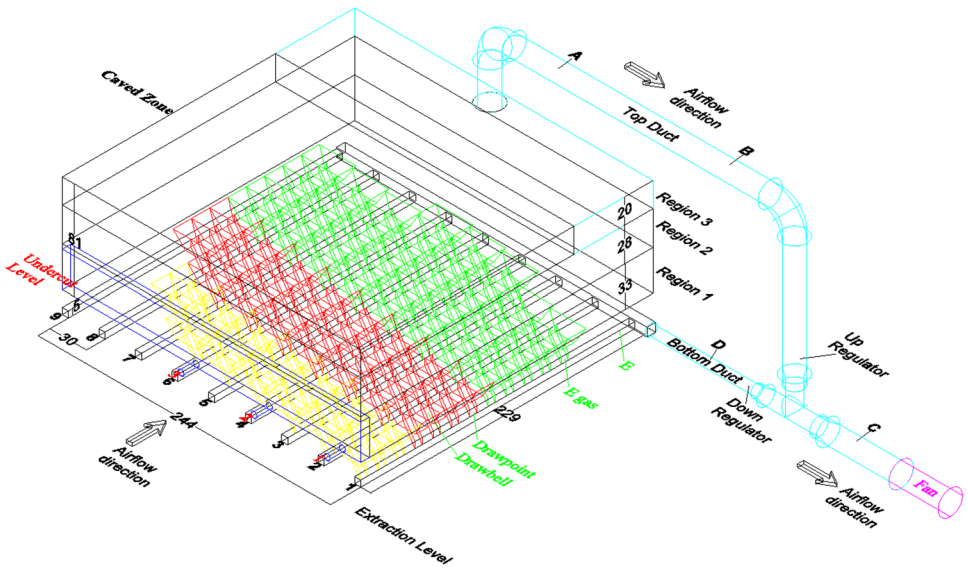

Fig. 1 Schematic diagram of the experimental model setup (unit: cm)

Case 1 Case 2 Case 3

Fig. 3 Three caved material cases

C 1: 100%+100% **C 2**: 100%+50% **C 3**: 25%+100% **C 4**: 6.25%+100%

Fig. 4 Four regulator combinations

an exhaust fan. The caved zone with a full dimension of 229 cm × 244 cm × 81 cm was separated into three vertical regions (Regions 1, 2, 3); the extraction level consisted of nine parallel drifts with a dimension of 5 cm × 5 cm at a distance of 30 cm (center to center distance between the drifts), and 188 drawpoints with an El Teniente layout; the undercut level comprised of three 5-cm-diameter drifts (undercut drifts could be clogged with duck tape); and 94 drawbells (30 cm high) served as the vertical connection between the caved zone and the extraction level, and each drawbell was connected to two drawpoints (shown in yellow, red, and green in Fig. 1). All extraction drift outlets merged into a 10-cm-diameter PVC pipe; the top of the cave connected to another 20-cm-diameter duct. We arranged a 20-cm regulator in the top duct and a 10-cm regulator in the bottom pipe, referred to as *upregulator* and *downregulator*, respectively. A 15-cm T connector was utilized to connect the bottom and top ducts to the exhaust centrifugal fan with a 10 to 15 cm increaser and a 20 to 15 cm reducer, and 15 to 20 cm adaptor, respectively. A variable speed control device is used to control the centrifugal fan speed and simulate desired volume flow rates in the system.

To simulate the broken rock in a block cave mine and investigate the impact of rock properties on gas and airflow characteristics, we developed three different (material) cases by filling up the caved zone with various sizes of cardboard (cubic) boxes, as shown in Fig. 3. In all the three different cases, to simulate a caving process (cave evolution), different materials (different sizes of boxes) were used in Region 1, but keeping the same materials (same size boxes) in Regions 2 and 3. In Region 1, a mixture of 10-cm and 15-cm boxes (333 + 138), two layers of 15-cm boxes (242), and three layers of 10-cm boxes (741) were used in Case 1, Case 2, and Case 3, respectively. The upper two regions were consistent in three cases: two layers of 13-cm boxes (288) and one layer of 18-cm boxes (49). Based on the arrangement of boxes in the a bundle and a gap between the bundles, Case 2 seemed to have a relatively higher porosity, while Case 3 had a relatively lower porosity despite their identical height of 30 cm; the porosity in Case 1 was between Case 2 and Case 3.

Table 1 Regulator combination information

Combination (C)	Upregulator	Downregulator
1	100%	100%
2	100%	50%
3	25%	100%
4	6.25%	100%

% is the ratio (the percentage) of the open area over the regulator's cross-sectional area

As shown in Fig. 4, *up (gray/blue knob/valve)* and *downregulators (red valve)* were utilized for airflow distribution in the system. Table 1 presents blockage information about four regulator combinations. We achieved a *25%* opening of the *upregulator* by setting the valve opening at point 1 (point 6 is fully open) and further reduced it to a *6.25%* opening by adding a porous foam. As it was difficult to estimate the blockage of the porous foam, the opening area was assumed to be 5 cm in diameter in the CFD simulation. To investigate the impact of undercut drift openings, we prepared three 5-cm-diameter PVC pipes. To simulate the real-world condition of the broken rock and the gap between the broken rock and the undercut opening, we maintained the gap in the experiment

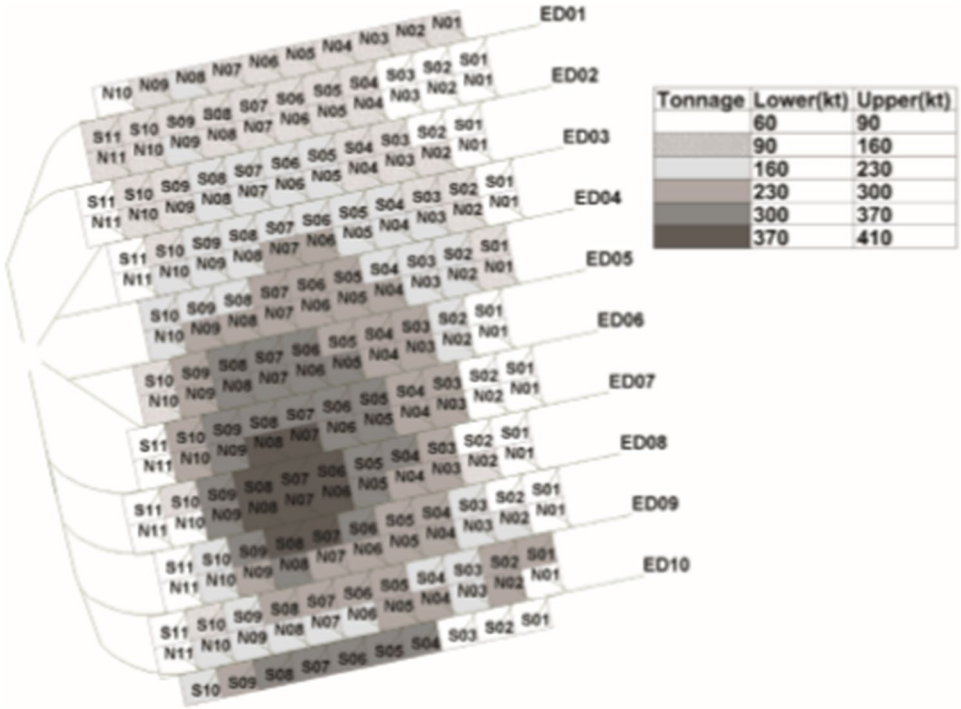

Fig. 5 Distribution of in situ tonnage and maturity within E48 cave. *Source*: Rahal et al. (2008)

S1: 94 (O) + 0 (C) **S2:** 72(O) + 22(C) **S3:** 52(O) + 42(C) **S4:** 21(O) + 73(C)

Fig. 6 Four cave footprints

by pulling the cover sheet a certain distance away from boxes; in the CFD simulation, we assumed this distance as 8 cm.

According to the distribution of in-situ tonnage and maturity within E48 Cave at the Northparkes mine displayed in Fig. 5, outer drawpoints terminated their service faster than relatively middle ones. Once becoming inactive, the drawpoints might be isolated (sealed) according to one of the Henderson mine's radon control measures [1]. Besides, some drawpoints might be disturbed by a sudden influx of nonporous and impermeable mud rush. As shown in Fig. 6, the obstructed areas were covered with transparent sheets, where the connections between the drawbells and production drifts were thwarted with duct tape. To examine the effect of various cave footprints on the cave airflow resistance, we investigated four scenarios of drawbells opening and closure under the material Case 2, as shown in Table 2. We obstructed undercut drift inlets and the *downregulator* during the experiment while keeping the *upregulator* fully open. Air entered through nine extraction drift inlets and exited through the exhaust duct.

Table 2 Drawbells opening and closure information

Scenario (S)	Drawbells (O, open)	Drawbells (C, closed)
1	94	0
2	72	22
3	52	42
4	21	73

Two transparent sheets (244 cm × 305 cm) were utilized to cover boxes, and duct tape is used to seal the sheet and the cave boundary properly to avoid leakage. While conducting

the experiment, we did not observe any movement of boxes and any expansion of flexible sheets due to the suction effect created by the exhaust ventilation system.

The fan is operated at four different settings: 70 V (pressure $P_{max}=215$ Pa, Airflow rate $Q_{max}=0.28$ m^3/s), 80 V ($P_{max}=270$ Pa, $Q_{max}=0.33$ m^3/s), 90 V ($P_{max}=310$ Pa, $Q_{max}=0.39$ m^3/s), and 100 V ($P_{max}=333$ Pa, $Q_{max}=0.44$ m^3/s). A hot wire anemometer with a range of 0.2–20 m/s and a resolution of 0.1 m/s and a fluke airflow meter with a range of −4000 to 4000 Pa and a resolution of 0.25 Pa were utilized for air velocity and pressure measurements.

By examining the velocity contours simulated using CFD, we explored suitable locations for taking air velocity and pressure measurements in the model. As shown in Fig. 7 (under the 70 V for Case 3), Point *A*, after the bend, was not appropriate for velocity measurement as the center position could not represent the average airflow through the duct; while Point *C*, after regulators, was not a proper location where higher velocities were in the lower portion of the duct. Since the measurement devices were sensitive to the airflow direction, a turbulent flow pattern could result in unreliable data [34]. Considering the Reynolds number of more than 10,000 within both ducts, the method factor was calculated as 0.8. The airflow rate was calculated as the product of velocity, inner duct area, and the method factor. The airflow rate through Point *C*'s cross-section was calculated as a sum of the flow rates through both ducts (A and B). We also measured air velocities near undercut and extraction drift inlets.

We prepared three cases to investigate various caved materials, arranged four regulator combinations to explore the airflow distribution, and developed undercut drift openings and closures to study the structure change. In total, we had 112 sets of experimental data considering four cave footprint scenarios. Every set of data was measured two times, and the average value was utilized for data analysis.

2.2 Numerical Model Setup

A numerical model was developed for a comparative study and airflow behavior through the flow domain was analyzed using a CFD software package, scFLOW, developed by Cradle Software Company. We utilized a fan model function in the CFD simulation, which required *P-Q* information (70 V, 80 V, 90 V, and 100 V) from the experimental results. We also utilized a porous media function in the CFD simulation, which required particle size, porosity, and shape factor; we set the porosity as 5% for three layers of 10-cm boxes (Case 3), 20% for two layers of 15-cm boxes (Case 2), and 8% for the combination case (Case 1); the shape factor was 1 for all three cases. In the model, we set the area from the fan towards the cave system as upstream, which indicates the air was exhausted. The outlet was modeled as a natural in/outflow condition, and extraction drift inlets were set as the zero static pressure conditions. Undercut inlets were modeled as the zero static pressure conditions when the drifts were open; otherwise, they were set to be the wall conditions. All simulations were conducted under a steady-state analysis. Considering three material cases, four fan operating conditions, two undercut drift situations, and four regulator combinations, we performed a total of 96 numerical simulations.

Before performing the CFD gas simulations, we have conducted laboratory experiments to generate the input data needed for CFD simulations. For these experiments, we used dry ice for CO_2 generation. Caldwell et al. [35] report that 5 lbs of dry ice can change into 3% of CO_2 per hour with the generation rate of 600 ml/min. With this background, for the CFD gas simulations, the generation location for CO_2 was assumed to be situated in the undercut inlets with the generation rate of 960 ml/s. The other source locations were assumed to be drawpoints with the generation rate of 600 ml/s. Hence, 188 drawpoints generated CO_2 evenly, assuming the worst-case scenario that the maximum number of machines working at all drawpoints. The steady-state analysis was chosen for gas simulations. Table 3 lists the six conditions of airflow rates through the system. The inlets considered the static pressure of zero conditions with an initial concentration of 0.04% CO_2 and a diffusion coefficient of 1.67×10^{-5} m^2/s, and the outlet considered a natural gas inflow/outflow condition.

For validation purposes, we used a small-sized fan with speed control. The CO_2 generation location was marked as *E gas*, as shown in Fig. 1 with a release rate of 960 ml/min, and the CO_2 concentration measurement was located at Point *E*.

3 Results and Discussion

3.1 Airflow Characteristics

In the *P-Q* characteristic curves and equations, the *P* refers to a static pressure difference between two points of interest; the *Q* refers to the airflow rate through the cross-section

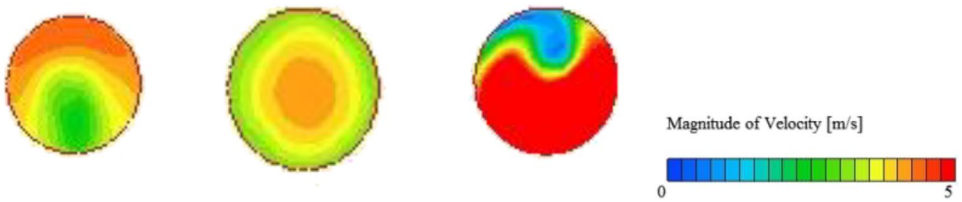

Fig. 7 Air velocity contours of the duct cross-sections at Points *A*, *B*, and *C* (20 cm diameter duct)

Table 3 Six conditions of the airflow rates through the system

Condition	The top duct (m^3/s)	The bottom duct (m^3/s)	Total (m^3/s)
1	0	0.1	0.1
2	0.02	0.1	0.12
3	0.04	0.1	0.14
4	0.03	0.07	0.1
5	0.05	0.05	0.1
6	0.07	0.03	0.1

where the measurement points are located in the system. At Point *C*, we used the average airflow (Q_a) at total inlets and outlets. The difference in airflow values between total inlets and outlets was attributed to the air leakage in the physical model. The *P-Q* curve slope represents the cave airflow resistance, and the index *n* value can provide useful information for the ventilation network analysis. The *No* condition represents the scenario of three undercut drift inlets' closure, and the *Three* indicates that three undercut drifts were open.

3.1.1 Effects of Regulator Installation and Undercut Structure

Figure 8 shows the effects of regulator installation and undercut structure on the cave airflow behavior for different material conditions. Under a certain regulator combination condition, the increment of fan speed gave rise to the pressure and airflow rate measured at Point *C*. Comparing slopes of *P-Q* curves, it can be observed that the use of regulators at either location decreased the total airflow rate through the system, increased the pressure, and escalated the airflow resistance within the system.

As shown in Table 4, under a given regulator combination, the higher percentage of air passed through the caved zone in Case 3 campared to Cases 1 and 2; regulators were

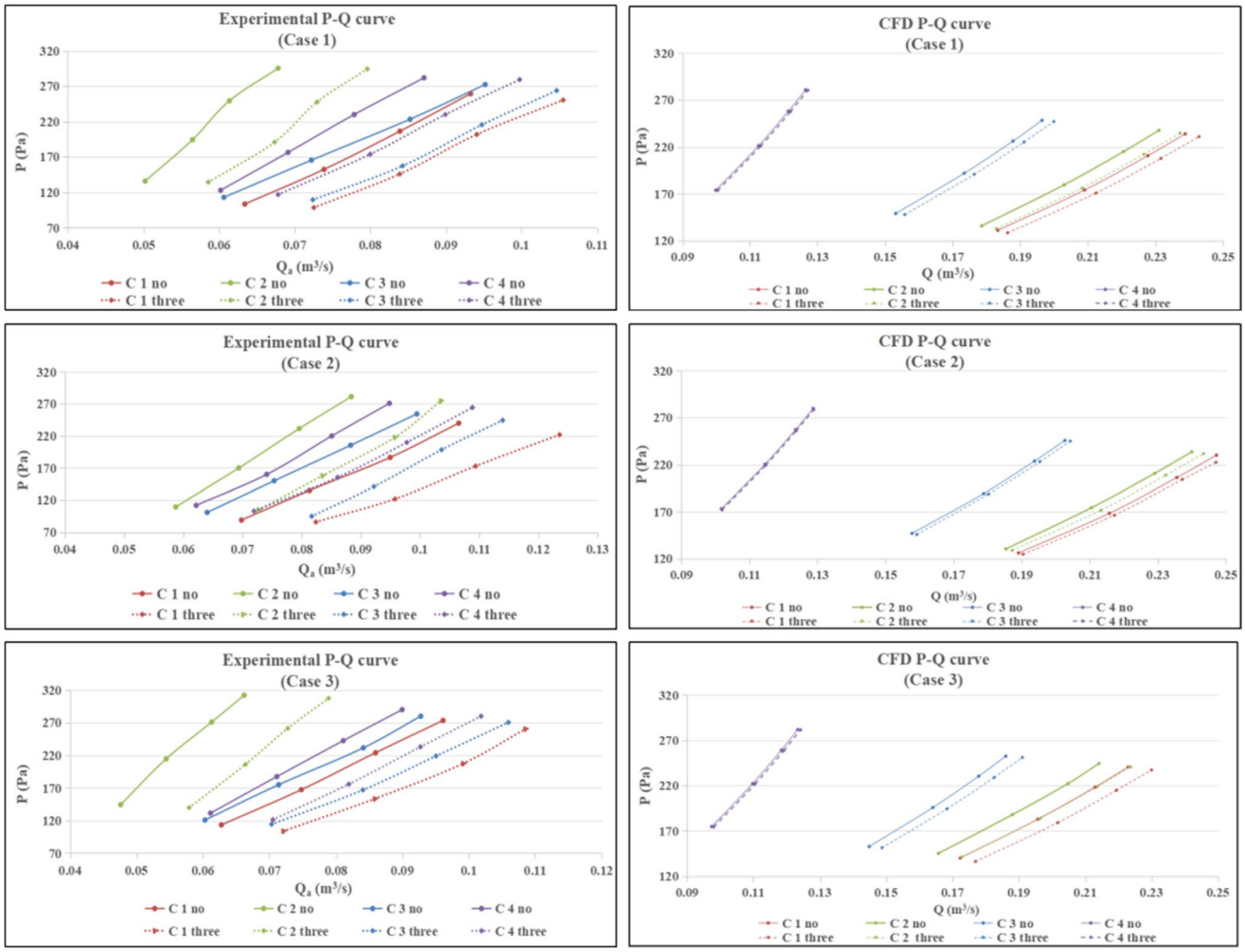

Fig. 8 *P-Q* curves under various regulator combinations and undercut structures at various material conditions

Table 4 Average percentage of airflow passing through the caved zone (%)

Case	Experimental data								CFD data							
	C 1		*C 2*		*C 3*		*C 4*		*C 1*		*C 2*		*C 3*		*C 4*	
	No	*Three*	*No*	*Three*	*No*	*Three*	*No*	*Three*	*No*	*Three*	*No*	*Three*	*No*	*Three*	*No*	*Three*
1	50.42	50.76	82.12	82.29	44.90	47.33	36.09	36.68	75.17	75.65	80.82	80.93	66.23	66.77	32.53	32.66
2	41.53	45.26	76.75	77.46	37.78	40.74	32.71	34.46	75.41	75.69	80.97	80.97	66.28	66.67	32.33	32.45
3	59.97	60.28	87.93	87.95	49.69	51.74	41.27	40.34	72.57	74.30	78.49	79.65	64.92	66.17	32.58	32.86

No denotes three undercut drifts are closed, *Three* denotes the drifts are open; *C* denotes regulator combination.

able to distribute airflow rates: the *upregulator* reduced while the *downregulator* increased the percentage of airflow rate through the caved zone. Undercut drift openings led to increased total airflow quantity through the system and airflow percentage through the caved zone in most cases, and reductions in airflow quantity through extraction drifts and system airflow resistance. Similar observations were confirmed in the CFD results except that the *6.25% + 100%* combination (C 4) while the *100% + 50%* (C 2) combination in the experimental data gave the highest cave airflow resistance among the four regulator combinations. The airflow rate, pressure, and *P-Q* curve slopes at Point *C* reflected the regulator installation information within the system.

The average *n* values at Point *C* were 2.20 and 2.44 for the experimental data with undercut drifts' closure and opening; and they were 2.10 and 2.11 for the CFD data. Both the experimental and CFD data confirmed a similar observation that the *n* value for undercut drifts' opening was higher than that for the closure.

3.1.2 Effects of Caved Materials and Undercut Structure

Figure 9 presents the effects of caved materials and undercut structure on the cave airflow characteristics at various regulator combinations. Under a given caved material condition, the increase of fan speed escalated the pressure and airflow rate measured at Point *B*; under a particular fan condition, Case 3 shows the lowest airflow rate and the highest pressure among three cases; undercut drifts' closure reduced airflow rate through the caved zone. Comparing slopes of *P-Q* curves, it can be observed that Case 3 offered the highest cave airflow resistance, followed by Case 1 and Case 2; undercut drifts' opening reduced the cave airflow resistance as they provided extra pathways for air through the cave. The fluctuation of *P-Q* at Point *B* will give indications about the changes in rock fragmentation within the cave; and the particle size distribution at drawpoints could be monitored to provide information for ventilation system design.

Though the CFD simulation results confirmed similar observations, the deviation from the experimental data in terms of the pressure and airflow rate is mainly due to the following elements: it was difficult to obtain an accurate estimation of porosity of the drawbell zone, mesh, and porous foams used for blocking connection in the physical model; discrete (physical) and continuum (numerical) models were different [11, 12].

The average values of *n* were 2.52 and 3.01 for the experimental data with undercut drifts' closure and the opening, and they were 2.02 and 2.06 for the CFD data. Undercut drifts' opening led to an increase of the index *n* value, which was observed in both experimental and CFD results.

The information at Point *D*, we could not observe the effect of the material combination based on *P-Q* curve slopes (cave airflow resistance) in the physical model, which was attributed to large size materials and the arrangement we utilized in the physical model, and the air was sucked down through the gaps between the boxes and outer sheets, instead of porous boxes; but we could observe the effect in the CFD model. As shown in Fig. 10, under material Case 1 and regulator C 2, undercut drifts' opening decreased the *P-Q* curve's slope; the index *n* values calculated were 2.03 and 2.17 for the closure and opening in the physical model, and they were 2.16 and 2.19 in the numerical model.

If the index *n* could reflect the difficulty of airflow through a system in the physical model, extraction drifts had made the air most difficult to move through the system, followed by the regulators and porous materials; however, in the CFD model, this sequence was porous materials, regulators, and extraction drifts. Undercut drifts had facilitated the airflow through the system in both experimental and CFD models.

The average standard deviations (variance) of the static pressure and air velocity at Point *C* were 1 Pa and 0.05 m/s, respectively; at Point *B* were 1 Pa and 0.06 m/s, respectively; and at Point *D* were 0.9 Pa and 0.07 m/s.

3.1.3 Effect of Cave Footprint

In reality, the number of active drawbells varies from hundreds to thousands in different cave mines, and it alternates during the operation within a single cave. Four scenarios were prepared to simulate the effect of various drawbell numbers (cave footprints) on cave airflow resistance. As shown in Fig. 11, S4 with the lowest active drawbell number

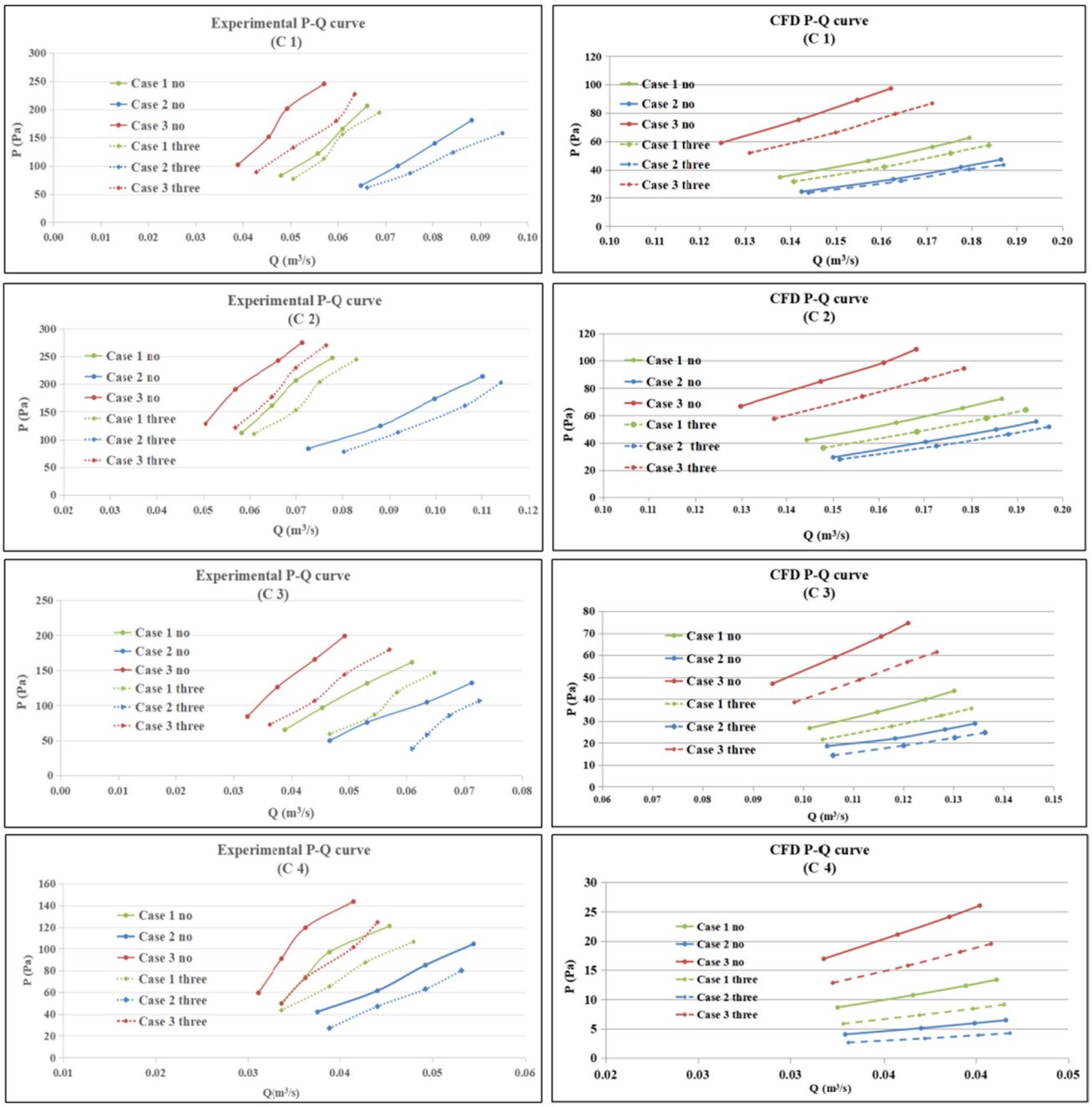

Fig. 9 *P-Q* curves under various materials and undercut structure at different regulator combinations

showed the highest cave airflow resistance among the four scenarios, which suggested that the shrinking/reduction (isolation) of the cave footprint might increase the cave airflow resistance. The *P-Q* information at Point *B* might reflect drawpoints isolation in the extraction level.

3.2 Gas Flow Characteristics

Figure 12 shows the air velocity contour through production drifts, and high-velocity magnitude located near the inlets and outlets of production drifts because of air loss through drawpoints in the middle portion of drifts. Figure 12 also displays the airflow pattern in the caved zone and the air exchange interaction between the production drifts and the caved zone. The observation of air gain from the caved zone at the last two drawbells explained the relatively higher air velocity near the outlets of production drifts. Nine points (1–9) close to production drifts' outlets show gas measurement locations in the CFD model.

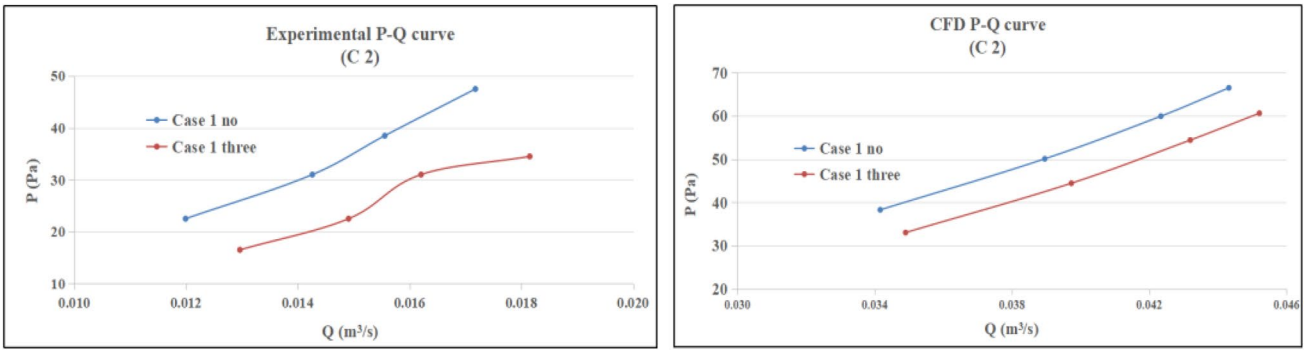

Fig. 10 P-Q curves at Point *D* under Case 2 and Case 1

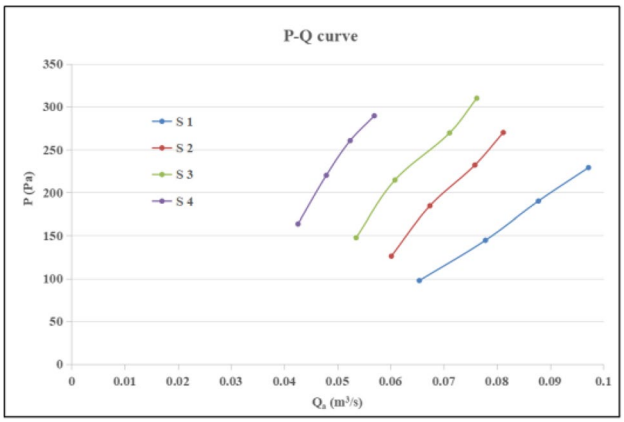

Fig. 11 Experimental *P-Q* curves under varying cave footprints

3.2.1 *CO_2 Distribution in the Extraction Level*

As shown in Fig. 13, under a specific ventilation configuration, the high CO_2 concentration area location was the outlets of the system (mainly near the outlets of extraction drifts 1 to 4); under Conditions 1, 2, and 3, it was observed that the increase of airflow rate through the system decreased CO_2 concentrations substantially in the extraction level since more air was involved into diluting the gas; while under Conditions 4, 5, and 6, the increase of airflow rate through the cave system might remove higher volumes of CO_2 generated in the cave and dropped CO_2 concentrations slightly in extraction drifts.

For designing a ventilation system of an underground mine with gas issues, instead of conducting the ventilation survey in the whole mine, some special areas could be given particular attention, or be monitored, or reversed ventilation can be considered to avoid build up of higher levels of gas in the system.

3.2.2 DPM Distribution in the Extraction Level

For experimental study in the lab, we used CO_2 as a pollutant source (to simulate DPM and airborne dust). As shown in Fig. 14, under a specific ventilation configuration, a high DPM concentration area is located

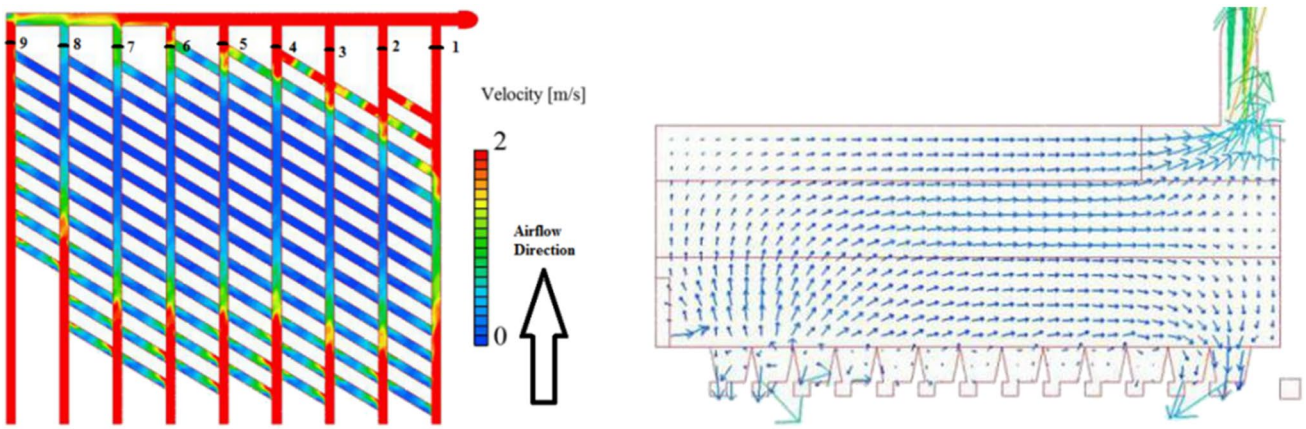

Fig. 12 Airflow distribution through extraction drifts and airflow vectors in the caved zone (cross-section located between production drift 5th and 6th)

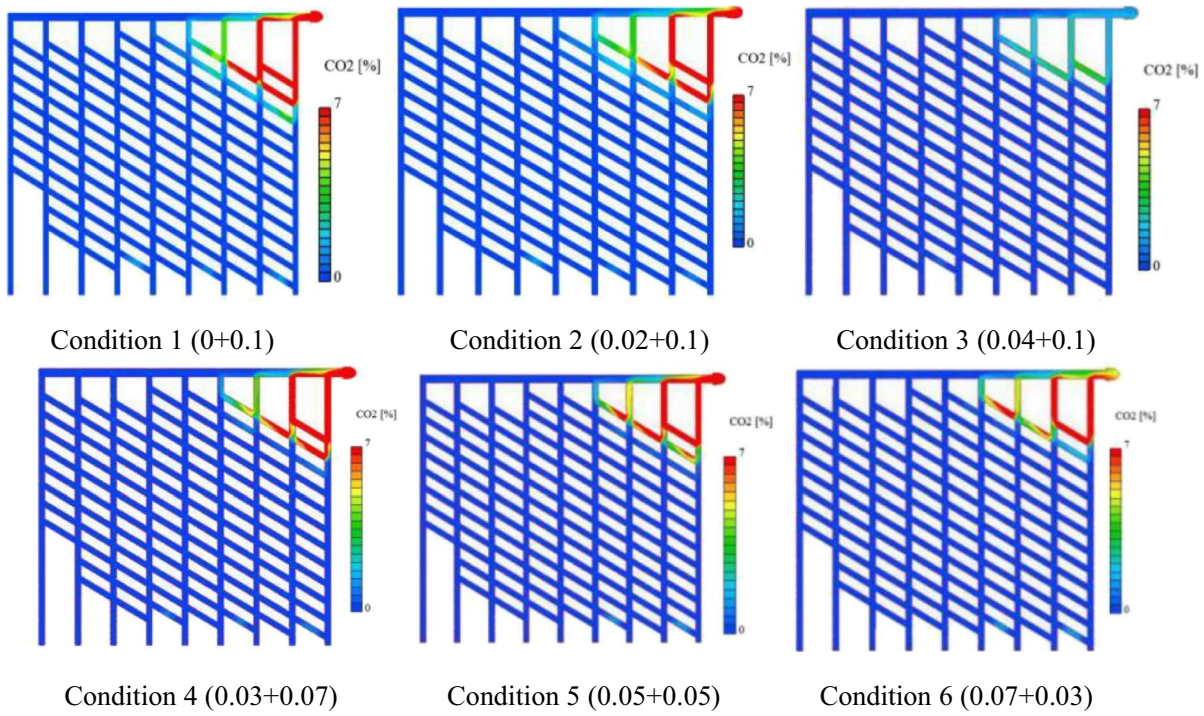

Fig. 13 CO_2 concentration distribution under varying airflow rate conditions

in the middle of extraction drifts due to the air loss into the caved zone; under Conditions 1, 2, and 3, the increase of airflow rate through the system decreased the high concentration area in the extraction level, while under Conditions 4, 5, and 6, the decrease of airflow rate through the extraction drifts escalated the DPM

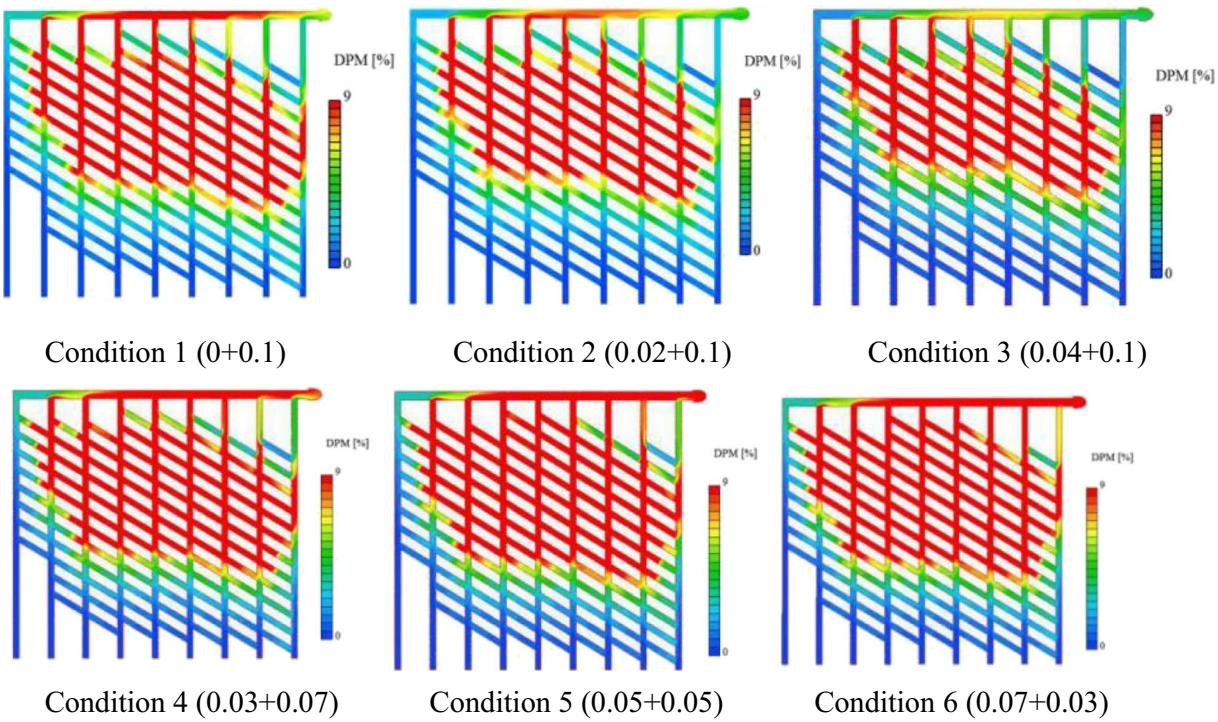

Fig. 14 DPM concentration contours under varying airflow rate conditions

Table 5 Gas concentrations (in %) at various locations and comparison with Condition 1

Item	Condition 1 (0 + 0.1) %		Condition 2 (0.02 + 0.1) % difference		Condition 3 (0.04 + 0.1) % difference		Condition 4 (0.03 + 0.07) % difference		Condition 5 (0.05 + 0.05) % difference		Condition 6 (0.07 + 0.03) % difference	
	CO_2	DPM	CO_2	DPM	CO_2	DPM	CO_2	DPM	CO_2	DPM	CO_2	DPM
1	20.93	3.54	19.17	25.13	92.26	38.18	− 18.71	− 20.77	− 4.38	− 46.65	49.76	− 97.68
2	11.28	4.55	29.25	20.47	79.34	35.32	− 25.22	− 29.65	− 42.26	− 67.97	13.95	− 151.70
3	3.78	6.37	24.76	19.18	49.72	33.20	− 13.72	− 34.78	− 45.35	− 77.37	− 35.94	− 170.14
4	1.30	8.09	14.66	16.52	34.65	28.92	− 6.58	− 42.49	− 38.30	− 95.70	− 105.98	− 208.47
5	0.31	10.73	25.70	15.59	43.76	27.47	30.84	− 44.21	53.24	− 104.21	47.73	− 251.51
6	0.09	16.52	14.88	17.38	34.84	30.12	− 18.72	− 39.18	16.01	− 93.27	17.05	− 234.06
7	0.06	16.66	24.29	15.45	31.23	26.38	− 38.79	− 50.17	− 6.75	− 125.25	3.22	− 327.06
8	0.05	16.97	17.84	16.51	25.64	28.62	− 29.73	− 41.62	− 3.65	− 84.44	− 0.53	− 113.56
9	0.05	2.80	7.53	24.54	21.44	39.53	0.19	− 5.10	11.56	-8.96	6.03	− 11.93
		Average	19.79	18.97	45.88	31.97	− 13.38	− 34.22	− 6.65	− 78.20	− 0.52	− 174.01

concentrations, even though the increase of airflow rate in the cave could remove more DPM through the top duct. The exhaust system with regulators might not be a practical solution for dilution of DPM in the extraction level.

As shown in Table 5, we selected 9 points located 10 cm away from the drift's outlets presented in Fig. 12 to check gas concentrations under various airflow rate combinations. Comparing with Condition 1, we observed significant decreases in the CO_2 and DPM concentrations under Conditions 2 and 3; and we also observed substantial increases under Conditions 4, 5, and 6.

The increase of the total airflow rate (using multiple fans) through the system favors the gas dilution, while under a given airflow rate (using multiple regulators), the CO_2 concentration in some locations might be reduced by increasing the airflow rate in the caved zone. However, the DPM concentration increased substantially with the reduction of airflow in extraction drifts.

For the experimental validation, the CO_2 concentration was measured at location *E Gas* under varying airflow rates with the CO_2 release rate of 960 ml/min. When the airflow rate through all the inlets increased from 0.0055 to 0.018 m^3/s, CO_2 concentrations monitored at Point *E* decreased from 0.55 ~ 0.6% to 0.3%, which indicated that the increase of airflow rate would reduce the gas concentrations.

4 Conclusions

This study investigated the effects of material combination, undercut structure, cave footprint, and regulators on the cave airflow resistance. Regulators were able to distribute airflow rates through the caved zone and extraction drifts. Bends and regulators made it challenging to obtain constant air velocity within the ducts. Gas experiment through the physical model is difficult due to the model size, air leakage, and lab environment.

Both the experimental and CFD simulation results demonstrated that the increment of porosity and particle size in the caved materials increases the area available for flow within the cave (decreased airflow resistance) and increased airflow distribution percentage through the cave system under a given regulator combination. The shrinkage/reduction of cave footprint decreases the area available for flow within the cave (increased cave airflow resistance) significantly. The undercut drifts' opening decreased the cave airflow resistance and escalated the index *n* value at various locations. The use of regulators increased the fan head pressure, decreased the overall airflow rate, and changed the distribution of airflow rates through the cave system and extraction drifts. The increase of airflow rate through the system is favorable for gas dilution regardless of the source locations; while the regulated airflow system might deteriorate gas dilution performance especially when the source is located in the extraction level.

At an operating mine, the particle size of caved materials, distribution of rock size exploited from drawpoints, and cave footprint alternation should be monitored as these are the basis for porosity change and cave airflow resistance. The study shows that the gas concentration in extraction drifts can be above the desired limit. The gas concentration in the extraction drifts should be monitored and correlated with the characteristics of ore and waste material within cave. Ventilation should be adjusted according to the dynamics of the caving process and various locations of gas resources. The findings from this study provide useful information for the optimization of a ventilation system in a block cave mine.

Declarations

Conflict of Interest The authors declare no competing interests.

References

1. Loring D and E Meisburger IV, (2010)*A discussion of radon and the mitigation strategy at the Henderson Mine*.
2. Loring D. and B. Nelson. (2006) *Transition of the Henderson mine ventilation system to the new lower levels*. in *11 th US/North American Mine Ventilation Symposium 2006*.
3. Loring DM et al. (2015) *A discussion of the automated ventilation systems at the Henderson mine*. in *15th North American Mine Ventilation Symposium*. Virginia, USA.
4. Brake D. (2013) *Fire modelling in underground mines using Ventsim Visual VentFIRE Software*. in *Proceedings of the Australian mine ventilation conference, Adelaide, SA, Australia*. 2013.
5. De Souza E (2015) *Cost saving strategies in mine ventilation*. in *Canadian Institute of Mining, Metallurgy and Petroleum (CIM) 2015 Convention, Montreal*.
6. Baysal A et al. (2017) *Prediction of airflow resistance of a matured panel cave*. in *16th North American Mine Ventilation Symposium*. Golden.
7. Pan Y, A. Jha and P. Tukkaraja. (2018) *An investigation of the effects of particle size, porosity, and cave size on the airflow resistance of a block/panel cave*. Proceedings of the 11th International Mine Ventilation Congress.
8. Bhargava R et al (2021) *Airflow characteristic curves for a mature block cave mine*. CRC Press: London. p. 56–64.
9. Erogul D et al (2017) *Evaluation of cave airflow resistance associated with multiple air gap geometries during cave evolution*. in *16th North American Mine Ventilation Symposium*. Golden.
10. Erogul D et al (2015) *Effect of the air gap associated with cave evolution on cave resistance*. in *15th North American Mine Ventilation Symposium*. Blackburg.
11. Ajayi KM et al (2019) Prediction of airway resistance in panel cave mines using a discrete and continuum model. Int J Min Sci Technol 29(5):781–784
12. Ajayi K et al (2019) Numerical investigation of the effectiveness of radon control measures in cave mines. Int J Min Sci Technol 29(3):469–475
13. Rahal D, J Dudley, and G Hout (2008) *Developing an optimised production forecast at Northparkes E48 mine using MILP*. in *5th International Conference and Exhibition on Mass Mining, Luleå, Sweden*. 2008.
14. Botha J, Arkadius SWT, Samosir E (2008) *Simulation applications at PT Freeport Indonesia's DOZ / ESZ block cave mine*. Lulea, Sweden.
15. Rajabipour A et al (2001) *Airflow resistance in walnuts*.
16. Tabil LG et al (2003) Airflow resistance of sugarbeet. J Sugar Beet Res 40(3):67–86
17. Reed S et al (2001) Resistance of marigold flowers to airflow. Trans ASAE 44(3):639
18. Kashaninejad M, Tabil L (2009) Resistance of bulk pistachio nuts (Ohadi variety) to airflow. J Food Eng 90(1):104–109
19. Shahbazi F (2011) Resistance of bulk chickpea seeds to airflow. J Agric Sci Technol 13(5):665–676
20. Kenghe R et al (2012) *Airflow resistance in soybean.* International Agrophysics. **26**(2).
21. Agullo J, Marenya M (2005) Airflow resistance of parchment arabica coffee. Biosys Eng 91(2):149–156
22. Sacilik K (2004) Resistance of bulk poppy seeds to airflow. Biosys Eng 89(4):435–443
23. Rueda N (2017) *Co-simulation: 1D to 3D coupling in an underground mine ventilation simulated model*. in *16th North American Mine Ventilation Symposium*.
24. Fava HZL et al (2019) *Hybrid CFD-network methodology for improved DPM modelling*.
25. Pan Y et al (2021) Investigation of airflow characteristics under parallel fan conditions in a block cave mine. CIM J 12(4):169–178
26. Sakoda A, Ishimori Y, Yamaoka K (2011) A comprehensive review of radon emanation measurements for mineral, rock, soil, mill tailing and fly ash. Appl Radiat Isot 69(10):1422–1435
27. Bhargava R et al (2018) *CFD analysis of the effect of porosity, quantity and emanating power variation on gas emissions in block/panel cave mines*. Proceedings of the 11th International Mine Ventilation Congress.
28. Ajayi K et al (2015) *Computational fluid dynamics study of radon gas migration in a block caving mine*. in *15th North American Mine Ventilation Symposium*.
29. Wallace K, Prosser B, Stinnette JD (2015) The practice of mine ventilation engineering. Int J Min Sci Technol 25(2):165–169
30. Zheng Y (2011) *Diesel particulate matter dispersion analysis in underground metal/nonmetal mines using computational fluid dynamics*, Missouri University of Science and Technology.
31. Kumar A (2019) *Dust transportation and settling within the mine ventilation network*.
32. Jha A et al (2021) *Scale model investigation of ventilation parameters in a block cave mine*. CRC Press: London. p. 556–562.
33. McPherson MJ (1993) *Subsurface ventilation engineering*. 1993. p. 18–20.
34. Hartman HL. et al (1997) *Mine ventilation and air conditioning*. Third ed.: John Wiley & Sons.
35. Caldwell DC et al (2006) *The sublimation rate of dry ice packaged in commonly used quantities by the air cargo industry*, FEDERAL AVIATION ADMINISTRATION OKLAHOMA CITY OK CIVIL AEROMEDICAL INST.